J Mater Sci (2012) 47:55–67
DOI 10.1007/s10853-011-5915-8

ANNIVERSARY REVIEW

Size effect on stability of shear-band propagation in bulk metallic glasses: an overview

Y. Yang · C. T. Liu

Received: 17 June 2011 / Accepted: 27 August 2011 / Published online: 13 September 2011
© Springer Science+Business Media, LLC 2011

Abstract Understanding of the size effect on shear banding in bulk metallic glasses (BMGs) is currently the topic of active research but also remains under intense debates. In this article, we provide an overview of the recent research findings from experiments, theoretical modeling, and atomistic/continuum simulations which are intended to advance our knowledge related to the size effect on the stability of shear-band propagation in BMGs. Through the compilation of and comparison among the results reported in the literature, we aim at providing a comprehensive understanding of the underlying mechanisms and a unified physical picture of the size effect on shear-band propagation and its resultant ductility in BMGs.

Introduction

Bulk metallic glasses (BMGs) are alloys without long-range translational order [1]. As compared to their crystalline counterparts, they possess much higher mechanical strengths and corrosion resistance owing to the lack of dislocation-like crystalline defects [2–5]. However, they are also plagued by their structural amorphousness and usually exhibit brittle-like failure under uniaxial loading [6]. One common failure mode is the instant shear-off failure along an inclined shear plane upon yielding, which makes BMGs unsuitable for structural applications, at least at the current moment, despite their merits in other mechanical attributes [2].

The apparent origin of brittleness in BMGs is the catastrophic propagation of shear bands, which are a planar defect with a thickness varying from $\sim$10 to $\sim$100 nm [7–11]. In the literature, the shear-band nucleation is ascribed to the inelastic motion and coalescence of some basic 'flow unit' intrinsic to BMGs [12–15], which was modeled as either free-volume [12] or shear transformation zone (STZ) [13]. In the original free-volume model, a vacancy-like atomic-scale defect was assumed, which could allow an atom to jump in and out of without changing the material's potential for the accommodation of inelastic deformation; while in the STZ model, a shear intensified region consisting of tens or hundreds of atoms was conjectured, which behaves as an analog of dislocation to carry the plastic flow in BMGs. Regardless of the details of the atomistic models, shear banding takes place as the otherwise isolated shear of the basic flow units becomes highly correlated and concentrated at a low temperature and a high mechanical stress [12, 13, 16, 17]. Once this occurs to BMGs, a shear band forms as a banded region where the subsequent plastic flows are concentrated. In the majority of uniaxial tests, it is the flow concentration and catastrophic shear-band propagation that lead to the brittle-like failure in BMGs.

As the macroscopic plastic flows are accommodated by shear bands, much of the research efforts have been directed to the understanding of their behaviors, such as the measurement of the temperature rise within shear bands [18–20] and the shear-band velocities [21, 22], the simulation of shear banding from either the atomistic or continuum aspect [16, 17, 23], and the theoretical modeling of

Y. Yang (✉)
Department of Mechanical Engineering,
The Hong Kong Polytechnic University,
Hung Hom, Kowloon, Hong Kong
e-mail: mmyyang@polyu.edu.hk

C. T. Liu
Research Center of Advanced Structural Materials,
Department of Mechanical and Biomedical Engineering,
City University of Hong Kong, Tat Chee Avenue, Kowloon,
Hong Kong

shear banding with a size effect considered [24–29]. Despite the enormous research efforts devoted so far, drastically different results were reported from different research groups which may contradict each other, and different models have been proposed which may succeed in explaining some aspects of the shear-banding behavior but fail in others. In this article, we aim at providing a comprehensive overview encompassing the recent findings related to the size effect on shear-band propagation in BMGs, through which we hope that more insights could be stimulated for a better understanding of the complex shear-band propagation behavior and the resultant ductility in BMGs.

Origin of size effect

At a low stress or high temperature, BMGs deform via the isolated shear of their basic flow units at the atomic scale [12–14, 17]. While the original free-volume model has been widely used previously by the scientific community to rationalize the deformation behavior of BMGs [12], criticisms have also been raised against the physical ground for the existence of such a vacancy-like free-volume defect in BMGs [30], of which the original proposal came from the notion of hard-sphere packing for constructing an amorphous structure. However, for BMGs with metallic bonds, atoms behave essentially like 'elastic spheres', which could be squeezed and sheared without the assistance of any vacancy-like defects. Through a variety of structural studies [31–34], it was proposed that the amorphous structure of BMGs can be simply viewed as a composite of three 'ingredient' regions with different characteristic bond lengths, i.e., the regions of atoms with long, intermediate, and short bonds (Fig. 1a–d), and it was further suggested that the free-volume may be referred to as the regions of long atomic bonds that can cause structural dilatation under shear [30, 34]. From this regard, free-volume is not a vacancy-like defect in BMGs but can be understood as a zone of loosely packed atoms. This new concept of 'free-volume zone' shares a similar physical implication with the classic STZ theory on the mechanical deformation of BMGs [13], and conforms to the recent findings on their structural characteristics [31, 32]. Furthermore, it sheds new light on the nucleation of shear bands, which does not demand the break-down of tightly bonded atomic clusters but seeks a path of the least resistance, which may be the interconnection or transition regions that bridge the tightly bonded atomic clusters encaging the isolated free-volume zones (Fig. 1d) [35].

To nucleate a shear band, it can be envisaged that a sufficient number of free-volume zones needs to be joined together for the formation of a shear-band embryo, where strain localization starts to emerge [17, 34], and that its subsequent growth then triggers the macroscopic yielding in BMGs. Before the shear-band embryo evolves into a bona fide shear band, the micro-scale yielding in BMGs can be viewed as a continuous 'damaging' process entailing the percolation of free-volume zones [36]. However, as the shear-band embryo grows to a critical length, a shear instability event takes place, leading to the spring-back of the non-shear-banded region in BMGs [26, 37] and accompanied by a size effect on the subsequent propagation of the bona fide shear band [26, 38]. Here it should be noted that there could be two types of size effect associated with shear banding in BMGs. First, one can conceive that if a sample size is sufficiently small such that the shear-band embryo cannot be formed or grow to the point of instability, a mature shear band cannot nucleate [38], which corresponds to a deformation mode transition from the inhomogeneous to homogeneous plastic flow in BMGs. This intrinsic deformation mode transition may be also accompanied by a size effect on strength as suggested by Cheng [39], but the underlying physics still remains poorly understood at the current moment with contradictory results being reported [40–45]. In contrast, the second type of size effect is related to the shear-band propagation or the post-yielding behavior of BMGs, of which the phenomenology is more complicated and may not require a small-size sample to take effect [28, 29]. In our view, the majority of the size-effect phenomena reported in the literature may be categorized more appropriately as the size effect on shear-band propagation rather than nucleation. In what follows, we will focus on the topics associated with the size effect on shear-band propagation while leave those related to the size effect on shear-band nucleation as the future work.

Size effect on shear-band propagation

Progressive versus simultaneous shear

To begin with, let us discuss how a shear band propagates in a BMG and how a shear offset is formed due to shear-band propagation. In the literature, shear offset has been taken as a phenomenological variable to explain the size effect on the ductility of a BMG [24, 26]. Based on the experimental observations, one may propose a concept called the 'critical shear offset' (CSO) to rationalize this size effect [24], i.e., once a shear band produces a surface offset on a BMG within one shear operation exceeding the CSO, brittle-like shear-off failure occurs; otherwise, it remains stable after the cessation of the corresponding shear event. The repetition of the shear events then result in a serrated load–displacement curve as usually seen in

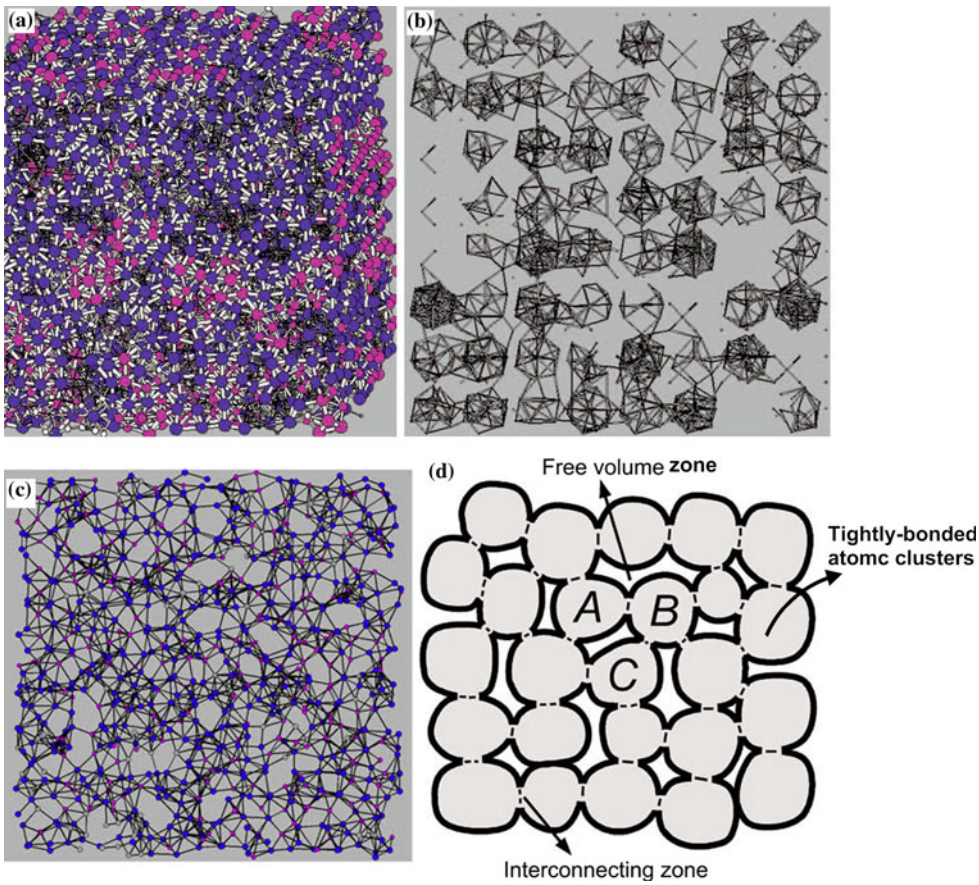

Fig. 1 **a** The three-dimensional amorphous structure constructed from Reverse Monte Carlo (RMC) simulations; **b** clusters of imperfect icosahedral and cubic forms extracted from **a**; **c** a layer inside the rebuilt three-dimensional atomic structure; and **d** the sketch of tightly bonded atomic clusters randomly and tightly connected to each other by interconnecting zones and separated by free-volume zones for a BMG. (Note that **a** and **b** are adapted from [33] while **c** and **d** from [34])

different types of mechanical tests, such as nanoindentation [19, 46], micro- and macro-compression [26, 47]. However, there could be two seemingly contradictory interpretations for the same process of shear-offset formation, i.e., the progressive versus simultaneous shear [21]. Accordingly, there exist two versions of 'mechanisms' that one may propose for formulating the size effect.

In the progressive shear model, a fracture-process zone is assumed being continuously pushed forward by a propagating shear front (Fig. 2a). As it reaches the outer surface of a BMG sample, the shear event ceases with a shear-offset emerging, which is similar to the case of dislocation gliding for the formation of a surface step. In such a case, the size of the CSO, λ_{CSO}, may be estimated as that of the fracture-process zone, which is $\lambda_{CSO} \sim K_c^2/E\sigma_y$ [48], where K_c, E, and σ_y denote the fracture toughness, elastic modulus and yield strength of a BMG, respectively. Using the archived experimental data, Yu et al. [49] estimated the size of the fracture-process zone for a variety of BMGs, ranging from $\sim$200 nm for Mg-based BMGs to $\sim$100 μm for Zr-based BMGs. This implies that, if the shear offset was indeed produced via a progressive shearing process, the higher is the fracture toughness of a BMG the more ductile it would appear when subjected to uniaxial loading. Nevertheless, the recent experimental results obtained by Gu et al. [50] just cast a doubt on the above reasoning.

In contrast, cooperative materials gliding along a shear plane is assumed in the simultaneous shear model for the formation of a shear offset, as shown in Fig. 2b. As this occurs to BMGs, extensive plastic flows could be accommodated even by a single shear band [26, 47]. However, it should be emphasized that the experimental evidence available to date which supports the above shearing model were provided only from compression tests [26, 47, 51], and it is an open question if shear bands still behave the same way in tension tests. Physically, the formation of a shear offset via simultaneous shearing is implicative of a multi-step shearing process in a BMG which is devoid of any pre-existing shear bands. At the very beginning, a shear plane has to be 'established' to prepare for the subsequent simultaneous shearing, from which a shear offset can result. If this was so, one could envisage two shearing velocities resulting from a same yielding process. The first is the speed of the propagating shear front or the wave speed, as shown in Fig. 2a and the second is the gliding speed of materials along the shear plane, as shown in Fig. 2b. In view of this, it is likely that the wave speed may be too high to be captured by conventional means, such as the use of strain gauges [21] or a high speed camera [22]; as such, it can be inferred that

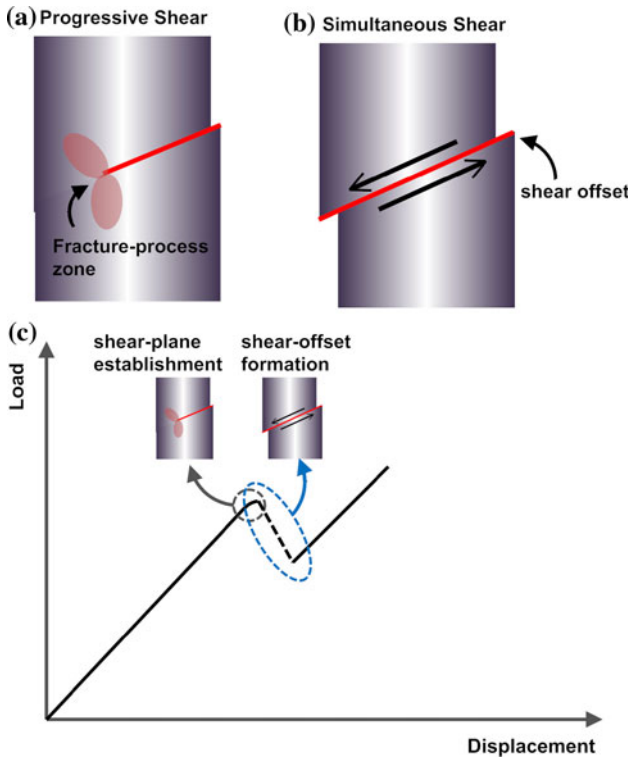

Fig. 2 The schematic illustrations of the **a** progressive and **b** simultaneous shear model for the formation of a shear offset; and **c** the sketch of a typical serrated load–displacement curve that is keyed to a sequence of shear-plane establishment and shear-offset formation under compressive loading

the reported shear-band speed may be more appropriately attached to the process of simultaneous shearing, which is relatively slow as entailing an inertial effect. In a regular compression test, it is hard to distinguish the two shearing processes from the load–displacement data because their signals partly overlap at the yielding point, as shown in Fig. 2c. However, with the acoustic emission (AE) technique, Vinogradov successfully detected the signal of the progressive shearing, which precedes that of the simultaneous shearing in a compression test [52]. A similar AE pattern was also reported by Dalla Torre et al. [53], which is supportive of the multistep feature of the shear-band propagation in BMGs under compression.

In nanoindentation of BMGs, a similar mechanism of multistep shearing was proposed by Packard et al. [54]. They noticed that the yield strengths of BMGs would be much overestimated in spherical nanoindentation if the signal of a displacement pop-in was mistakenly interpreted as an event of shear-band nucleation [54]. In view of this, they proposed a shear-plane criterion, arguing that a mature shear plane has to be formed before the pop-in. By adopting the shear-plane criterion, one can then obtain the yield strengths of BMGs from spherical nanoindentation with a similar magnitude as those from regular compression. Physically, the shear-plane criterion is consistent with a multistep shearing process and somewhat agrees with the previous findings from the examination of the AE signals. Apart from the experimental studies, Cao et al. [55] also investigated the shear-banding process in a BMG compression sample using the molecular dynamics (MDs) simulations. As compared with the experimental observations (Fig. 3a, b), their results showed the similar feature of shear-offset formation, which originates from a simultaneous shearing process after a shear plane penetrates and crosses the compression sample, causing local glass rejuvenation within the shear plane (Fig. 3c).

Size-affected malleability

After reviewing the findings on the mechanisms for shear-band propagation, we now turn to the study of the size effect on the compressive plasticity in BMGs. As widely observed in a variety of BMGs, people found that the smaller the samples are the more malleable they appear in compression tests [10, 24, 28, 29, 38, 42, 51, 56–60]. Likewise, there could be two competing views for modeling the size effect just like those for rationalizing the formation of a shear offset. Based on the principle of fracture mechanics, one can argue that the brittle-like failure corresponds to the instability of a shear band behaving as a crack-like defect. Once the elastic energy release rate at the shear front reaches a critical value, a brittle-like failure occurs; otherwise, the crack-like shear band remains stable within a BMG sample, leading to plastic deformation (Fig. 4a). As an alternative, one can also argue that the brittle-like failure results from the over-slip of a shear band, which is driven by the elastic energy released due to the spring-back of the testing machine and the non-shear-banded regions at the onset of yielding (Fig. 4b).

Han et al. [28] performed a systematic study of the size effect on the compressive ductility of a Zr-based BMG. In their work, a fracture-mechanics-based approach was utilized to formulate a criterion that governs the brittle-to-ductile transition in BMGs under compression. In doing so, the following shear-banding 'instability index', S, could be derived [28]:

$$S = \frac{\pi E D}{4\rho k_{\mathrm{M}}} = \frac{\pi E D^2}{4 H k_{\mathrm{M}}} \tag{1}$$

where E = the Young's modulus of a BMG; D = the diameter of a compression specimen; k_{M} = the machine stiffness; and ρ = the aspect ratio of the specimen height H to diameter D. Furthermore, Han et al. [28] proposed that there should exist an intrinsic index S_{c} for BMGs. The brittle-like failure takes place when $S > S_{\mathrm{c}}$; otherwise, extensive serrated plastic flows could occur with stabilized shear banding (Fig. 5a, b).

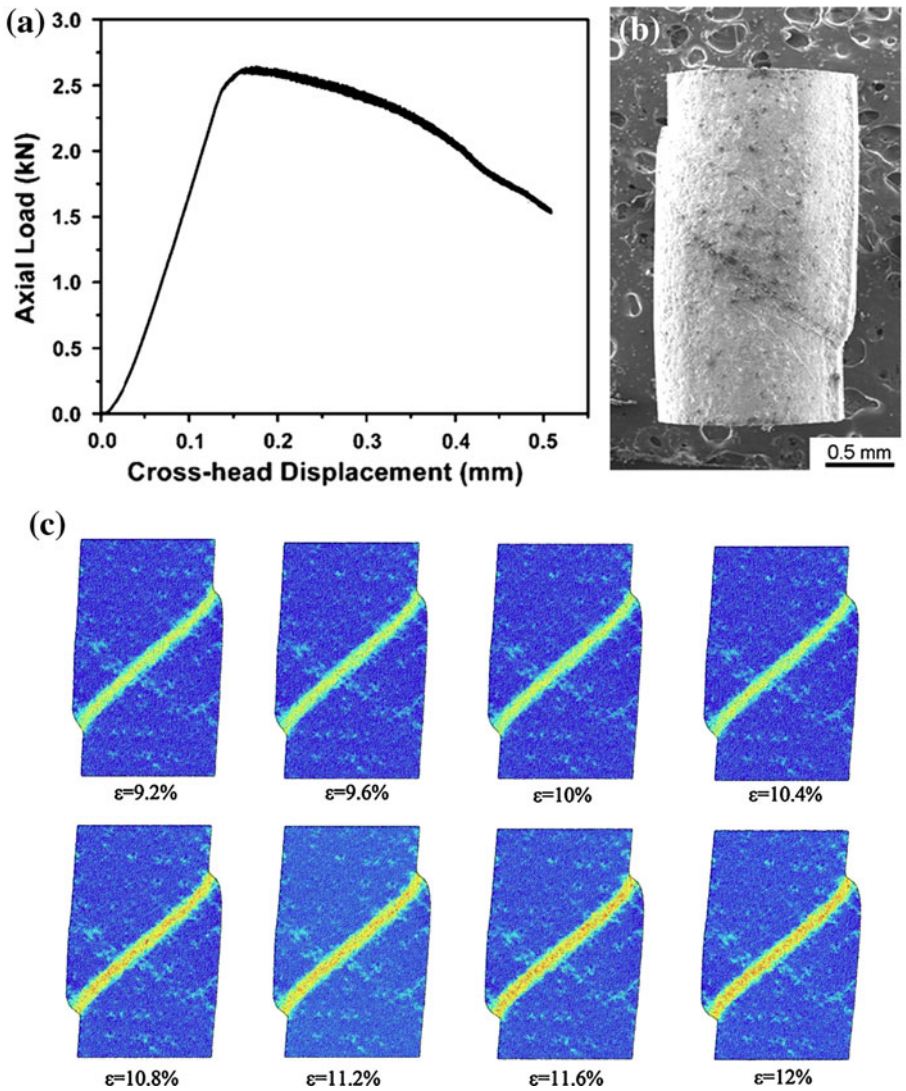

Fig. 3 **a** Axial load versus cross-head displacement for a small specimen having a diameter of 1.35 mm. The compression tests were interrupted following crosshead displacements of approximately 0.2 mm; **b** the morphology of the deformed compression specimen; and **c** the growth of the shear offsets on both sides of the sample, at larger overall sample strains ranging from $\varepsilon = 9.2$ to 12%, after the localization (deformation band) penetrates across the entire sample (Note that **a** and **b** are adapted from [51] and **c** from [55])

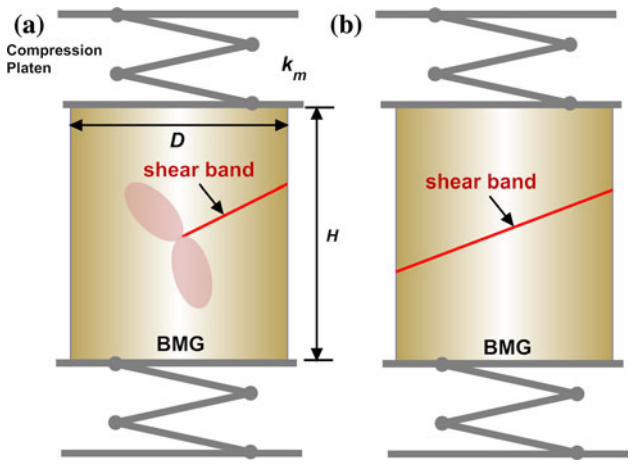

Fig. 4 The sketch of two types of models for formulating the dimension-induced brittle-to-ductile transition in BMGs under compression: **a** the fracture mechanics model and **b** the simultaneous slip model (Note that the springs represent the compression platens)

Note that the assumption of Han et al. [28] conforms to the physical process of progressive shearing. By comparison, one may develop a different 'size-effect' model based on the notion of simultaneous shearing [29, 56]. By simplifying the elastic support of a BMG compression sample as a spring (Fig. 4b), Cheng et al. [56] derived a new instability index S_{new}, which is:

$$S_{\text{new}} = H(1+S) = H + \left(\frac{\pi E}{4k_{\text{M}}}\right)D^2 \tag{2}$$

Following Han et al. [28], Cheng et al. also argued that the brittle-like fracture takes place when $S_{\text{new}} > S_{\text{c}}$ [56]. Regardless of the difference in the functional form, Eqs. 1 and 2 predict the similar trend of the machine-stiffness effect, that is, with the increasing machine stiffness, k_{M}, and the decreasing shear-band instability index S or S_{new}, shear banding tends to a more stable state under compressive loading.

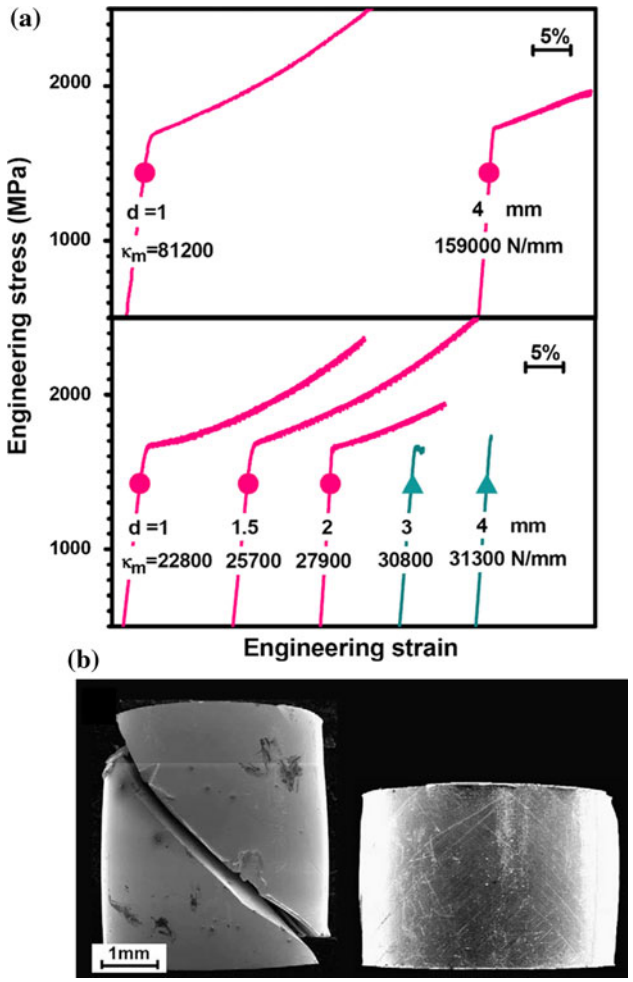

Fig. 5 **a** Engineering stress–strain curves of BMG samples measured for a range of controlled values of sample size and machine stiffness; **b** SEM micrographs of 4 mm 1:1 samples tested at a machine stiffness of (*left*) 31,300 N mm^{-1}, exhibiting an unstable behavior of shear banding by forming one dominant shear band, and (*right*) 159,000 N mm^{-1}, exhibiting a stable behavior of shear banding by forming dense shear bands, and thus uniform deformation, respectively (the figures are adapted from [28])

Undoubtedly, the shear-band instability index provides a convenient way to understand the machine-stiffness effect in BMGs. However, it is still not clear though of the structural origin for the brittle-to-ductile transition in BMGs, which is related to the material's intrinsic properties. Furthermore, the mechanical effect of the elastic support may be over-simplified as that of an elastic spring. Here, one can do a thought experiment. Suppose a BMG sample sitting on a half infinite space, such as in micro-compression tests [26], the 'machine' stiffness, i.e., the rigidity of the elastic substrate, now goes to infinity because of its unbounded size. In view of this, Eq. 1 then predicts a zero elastic energy transfer from the substrate and an always stable shear-banding scenario; while Eq. 2 predicts that only the height of a BMG sample matters for the size effect. However, physically, even when the size of the elastic support extends to infinity, spring-back will also occur locally underneath the BMG sample. Under compressive loading, the latter would behave like a punch indenting into an elastic substrate. As such, the elastic energy released from the elastic substrate cannot be zero at the onset of yielding. Some amount of elastic energies will still be transferred to the BMG sample through their contact area. As a result, the total elastic energy release should depend on the diameter of a BMG sample and the related size effect also involves the sample diameter.

Based on the consideration of energy balance, Yang et al. [29] derived the following criterion that involves two length scales for the size effect of BMGs:

$$L_{\text{ext}} = H + \alpha D \tag{3a}$$

$$L_{\text{int}} = \frac{2\Gamma_c}{E\varepsilon_Y^2 \sin\theta} \tag{3b}$$

Here L_{ext} is termed as the *extrinsic length scale* scaling with the elastic energy release from a bulk region; while L_{int} as the *intrinsic length scale* scaling with the critical plastic energy dissipation rate, Γ_c, on a shear plane, i.e., the plastic energy dissipation per unit area of a shear plane at the brittle-to-ductile transition. Presumably, this critical energy dissipation rate, Γ_c, should be only material dependent and could be accessed through testing different-sized BMG samples at a series of loading rates. Recently, Wu et al. [61] performed a size-effect study on three types of BMGs through regular compression tests. Interestingly, their results showed that the energy dissipation rate at the fracture point is size independent even though the measured malleability varies with sample size. To a certain extent, this finding suggests the plausibility of using a size-independent energy variable to interpret the size effect in BMGs, which is consistent with the notion of the critical energy dissipation rate as proposed by Yang et al. [29]. In Eq. 3a, α is a dimensionless factor being a function of the normalized elastic modulus and size of a BMG sample relative to those of its elastic support, and diminishing with the increasing support rigidity, of which the functional form may be derived using finite element (FE) simulations [26, 29, 60] (please see "Appendix" section for a further discussion of the α parameter); ε_y is the yield strain ($\sim$2%) of BMGs [62]; and θ is the shear-band inclination angle under compression ($\sim$42°) [63]. If L_{ext} is greater than L_{int}, the shear-band over-slips, causing an instant shear-off failure and sample fracture upon yielding; on the other hand, if L_{ext} is less than L_{int}, the shear-band slips in a jerky way dissipating the released elastic energy within a shear operation, leading to serrated plastic flows.

For the sake of comparison, one may construct a deformation map for the size effect with the above-mentioned

models. To this end, the equations for the size-effect models can be recast as follows for depicting the 'boundary' of the brittle-to-ductile transition:

$$\text{Han's Model [28]}: \quad H = \frac{\pi E D^2}{4 S_c k_M} \tag{4a}$$

$$\text{Cheng's Model [56]}: \quad H = S_c - \left(\frac{\pi E}{4k_M}\right) D^2 \tag{4b}$$

$$\text{Yang's Model [29]}: \quad H = \frac{2\Gamma_c}{E\varepsilon_Y^2 \sin\theta} - \alpha D \tag{4c}$$

As shown in Fig. 6a–b, all the models predict the similar trend of the machine-stiffness or substrate effect, the increase of which expands the stable shear-banding region, rendering BMGs with a greater ability to deform plastically in compression tests. However, Han's model predicts a reverse trend of the sample height effect as compared to the others. According to Han et al. [28], at a given sample diameter and machine stiffness, the higher is a BMG sample the more ductile would it appear. This predicted trend is somewhat contradictory to the reported experimental findings [29, 56, 60], which in turn implies that simply treating shear bands as cracks under compressive loading is not appropriate for BMGs, as also cautioned in Ref. [64].

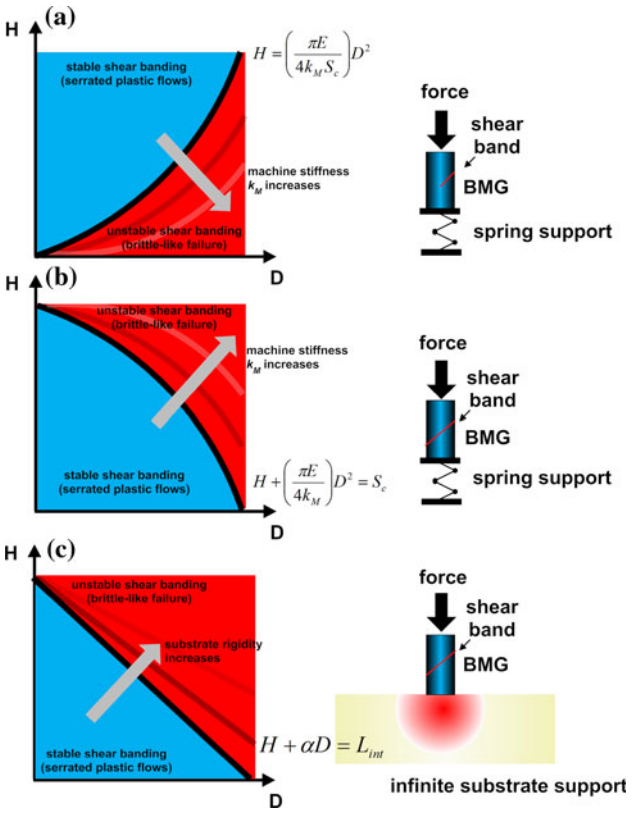

Fig. 6 The deformation mechanism map for the size effect in compression of BMGs constructed with the **a** Han's model [28], **b** Cheng's model, and **c** Yang's model for the case of α independent of D (Note that the cartoon to the *right* of the map illustrates the boundary condition and shear-band configuration used in different models)

Size-affected temperature rise within shear band

As the elastic energy is released to drive shear banding, it first goes to the plastic energy consumption and is then dissipated away completely or partially as heat, causing local temperature rise within the shear band. Since the elastic energy release is size dependent, it could be naturally conceived that this local temperature rise should be also size dependent. The size dependence of the temperature profile around a shear band has been foreseen in theoretical modeling [56, 65] and recently been experimentally verified by Miracle et al. [66]. To capture such a size effect, Cheng et al. [56] provides a simple model by assuming that the heat flux dumped into a shear band scales with the shear-band sliding speed and the strength reduction is proportional to the temperature rise on the shear plane. With these assumptions, the kinetic equation governing the vertical displacement, x, of a BMG compression sample can be cast as follows:

$$\frac{4M}{\pi D^2}\frac{\mathrm{d}^2 x}{\mathrm{d}t^2} = \left(\sigma_y - \frac{Ex}{H(1+S)}\right) - \left(\sigma_f - \frac{AE^2\varepsilon_Y \sin\theta}{2\rho c_p T_g \sqrt{\pi\alpha}} \int_0^t \frac{\mathrm{d}x}{\mathrm{d}t}(t-\tau)\frac{\mathrm{d}\tau}{\sqrt{\tau}}\right) \tag{5}$$

where M is the specimen's effective inertia; σ_y is the compressive yield strength; σ_f is the resistance of BMG at the onset of shearing; c_p is the heat capacity; ρ is the mass density; α is the thermal diffusivity; and T_g is the glass transition temperature. Solving Eq. 6a with the appropriate initial conditions $x(0) = 0$ and $\mathrm{d}x(0)/\mathrm{d}t = 0$ then gives the temperature rise within the shear band at a given size of a BMG sample and machine stiffness. Figure 7a–c show the typical results obtained by Cheng et al. for the BMG samples of a different size but with the same aspect ratio of 2:1 and machine stiffness, from which it can be seen that the sample diameter affects the vertical displacement x (the displacement jump caused by shear banding in compression tests), the temperature rise ΔT, and the vertical sliding speed $\mathrm{d}x/\mathrm{d}t$ of a shear band. As the sample diameter is increased, the peaks of the attainable temperature rise (Fig. 7c) and sliding speed (Fig. 7b) are raised. Accordingly, the vertical displacement jump is also widened, which generally agrees with the experimental findings (Fig. 7a).

Regarding the temperature rise in a shear band, a more general model was developed by Zhang et al. [65]. In Zhang's work, a shear band of a unit length is considered, which has a zero thickness and is subjected to a combination of shear and compressive stress. When the unit shear

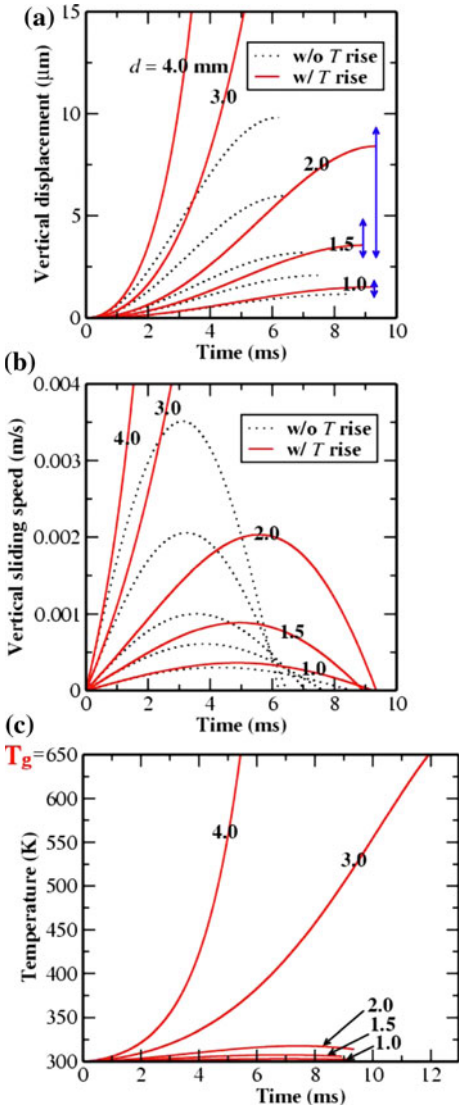

Fig. 7 Evolution of **a** vertical displacement (x), **b** vertical sliding speed, and **c** temperature in the shear band (T), all as a function of shear-band-sliding time t. *Solid lines* are model predictions with the T rise considered; *dotted lines* are model solutions without the T effect; *vertical bars* represent the range of experimentally measured step size for corresponding samples (see Ref. [56] for details) (Note that the figures are taken from Ref. [56])

band is sliding, unloading occurs within a shear relaxed region, which provides the local elastic energy release and evolves in thickness with the local strain rate, the local temperature rise ΔT, and the instantaneous shear offset, ψ, as shown in Fig. 8a. Here, the size effect manifests itself as the influence of the total shear offset, ψ_c, on ΔT. For modeling, a Mohr–Coulomb law was adopted for the yielding of BMGs and the reduction of the intrinsic yield strength was assumed due to a combined effect from the configurational change (ψ_c) and the local temperature rise (ΔT). Through the numerical simulation, some intriguing results were obtained, as shown in Fig. 8b, from which it can be clearly seen that the temperature rise within a shear band not only shows the dependence of shear offset (the size effect), but also is affected by the normal stress and strain rate (the details of the simulation have been described in Ref. [65]). At a low normal stress and a small shear offset, the strain rate effect can be neglected; however, it becomes non-negligible with the increasing normal stress and shear offset. The results of these modeling efforts are generally consistent with the experimental findings reported in the literature [18, 26, 56, 66]. For instance, Lewandowski et al. [18] devised the fusible coating method to measure the local temperature rise around the shear bands in the Zr-based bend bars, and reported that there could be a temperature surge of a few hundreds or even thousands of Kelvin increase when the shear bands hit the sample surface melting the tin coatings nearby; while from relatively small samples, the local temperature rise related to shear banding was reported insignificant [26, 56, 66]. On tensile testing of a Zr-based BMG, Liu et al. [67] also observed the melting of shear bands, and that molten droplets even flowed out of shear band cracks.

Intrinsic length scale for compressive plasticity

For crystalline metals, it would be straightforward to quote their ductility obtained from one sample size for their later structural use even at a much larger scale, since the dislocation-mediated plasticity is generally size insensitive at the macroscopic scale. However, it would be misleading if the material deformability measured at one sample size for BMGs were referred to as a size-independent 'intrinsic' property. Furthermore, even at the same sample size, the same BMG may exhibit different ductility with a different elastic boundary condition [28, 29, 56]. This complexity poses a serious question to us, i.e., how the intrinsic malleability of BMGs could be assessed and characterized. To address this question, we may now turn to the models developed for the size effect in BMGs [28, 29, 56]. In general, we may propose the following general criterion for the phenomenon of size-induced brittle-to-ductile transition in BMGs:

$$\text{Brittle-like failure: } L_{\text{ext}} > L_{\text{int}} \tag{6a}$$

$$\text{Serrated plastic flows: } L_{\text{ext}} \leq L_{\text{int}} \tag{6b}$$

in which:

$$L_{\text{ext}} = H + \tilde{\alpha} D^n \tag{6c}$$

$$L_{\text{int}} = \frac{2\Gamma_c}{E\varepsilon_Y^2 \sin\theta} \tag{6d}$$

where $\tilde{\alpha}$is a dimensionless factor accounting for the effect of the machine stiffness or the substrate rigidity but independent of the sample size; and the exponent n is a factor

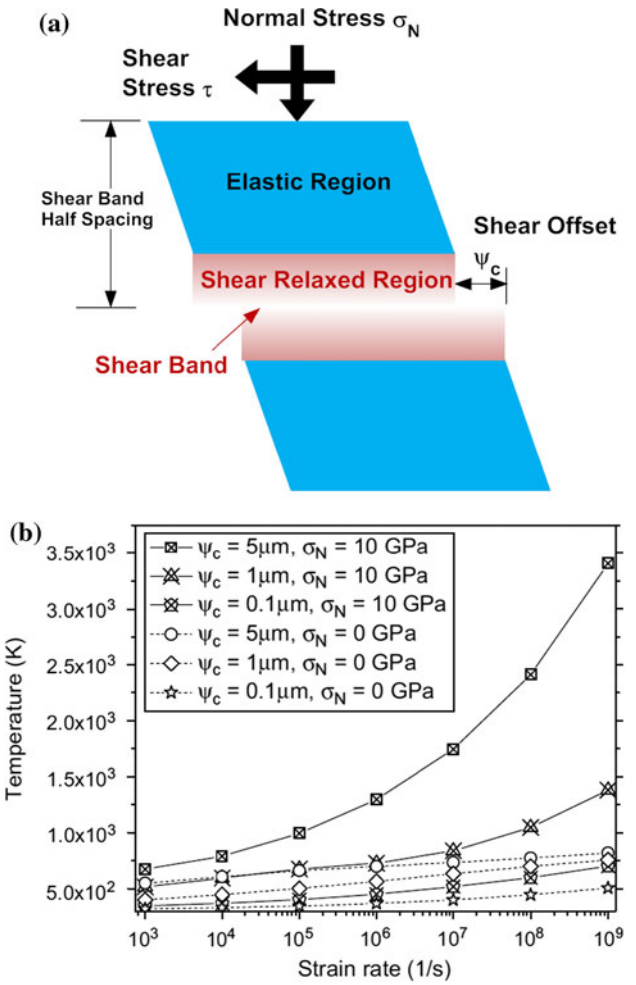

Fig. 8 **a** The sketch of the shear-band model developed by Zhang et al. and **b** the typical results showing the temperature rise in the shear band core as a function of strain rate, critical shear displacement, and normal stress. Note that normal stress has a higher influence on the temperature rise than strain rate (**b** is adapted from Ref. [65])

that accounts for the effect of the elastic boundary (=1 for a infinitely large elastic support as in microcompression [26], and =2 for a spring support as assumed for regular compression [56]). Equation 6c defines the extrinsic length scale L_{ext}, which can be experimentally manipulated; while Eq. 6d defines the intrinsic length scale, L_{int}, which is invariant with the testing environment and sample size, and provides a quantitative measure to assess the intrinsic deformability of BMGs.

As shown in Fig. 9a, the intrinsic length scale L_{int} dominates the size of the stable shear-banding region, while the extrinsic length scale L_{ext} mainly determines the shape of its boundary. For two types of BMGs, they may appear equally 'ductile' in small volumes; however, they will exhibit different failure behaviors as their size crosses the boundary of the size-induced ductile-to-brittle transition. For the so-called 'ductile' BMGs, they may possess a relatively large L_{int} and could therefore show plastic deformation even in a bulk form, such as the Zr-based BMGs with $L_{int} \sim 10$ mm (Fig. 9b); in contrast, for the so-called 'brittle' BMGs, they have a relatively small L_{int} and therefore, usually exhibit brittle-like failure in a bulk form, such as the Fe-based BMG with $L_{int} \sim 20$ μm (Fig. 9b).

From Eq. 6, it is evident that, to achieve desirable deformability, one need to have a BMG with a smaller shear-band inclination angle θ, a lower elastic limit ε_Y, a smaller Young's modulus E, and a higher critical energy dissipation rate, Γ_c. According to Sun et al. [68] and Zhao et al. [23], the shear-band inclination angle θ is related to the shear-induced dilatation, $\Delta v/v$, or the physical confinement of the loosely packed free-volume zones (or STZs) (Fig. 1d). A stronger confinement on free-volume zones leads to a lower volume dilatation, resulting in a smaller θ given that $\cot(2\theta) = -\left(\frac{\Delta v}{v}\right)/\dot{\gamma}$, where $\dot{\gamma}$ is the local shear strain rate [23]. In the literature, the ε_Y values were reported ranging from $\sim$0.014 to $\sim$0.022 [62], signifying the varying levels of difficulty in nucleating a shear band in BMGs. For a larger L_{int}, a lower ε_Y is preferred, which corresponds to a weaker resistance of BMGs against shear-band nucleation. Furthermore, the Young's modulus, E, of a BMG scales with its glass transition temperature T_g according to Ref. [69]. Therefore, if other conditions remain unaltered, lowering T_g is conducive to lengthening L_{int} and consequently ductilizing a BMG. Apart from those physical properties, the critical energy dissipation rate Γ_c, which denotes the ability of a shear band for absorbing mechanical energy, also plays an important role in determining L_{int}. Through the trends of the size-affected shear offset exhibited by different BMG micropillars, Yang et al. [60] recently uncovered that Zr- and Cu-based BMGs possess a stronger ability of energy dissipation than Mg- and Fe-based BMGs under compression, which may explain why some BMGs with an intermediate modulus appear more 'ductile' than those with a high or low modulus. Based on the above discussions, it is clear that there seems to be multiple routes one can employ for ductilizing BMGs, i.e., to expand the stable shear-banding region; however, each route may involve the tuning of the physical parameters in a collective way, which cause not only positive but also negative effects, leading to a trade-off. For instance, it is well known that BMGs with a high T_g or modulus tend to exhibit brittle failure under uniaxial loading, such as Fe-based BMGs, which may be explained as $L_{int} \sim 1/E$; however, the over-reduction of T_g may impair the energy dissipation ability (a low Γ_c) of a BMG, such as the Mg-based BMGs. As a consequence, the BMGs of a low modulus may also appear somewhat as brittle as those of a high modulus.

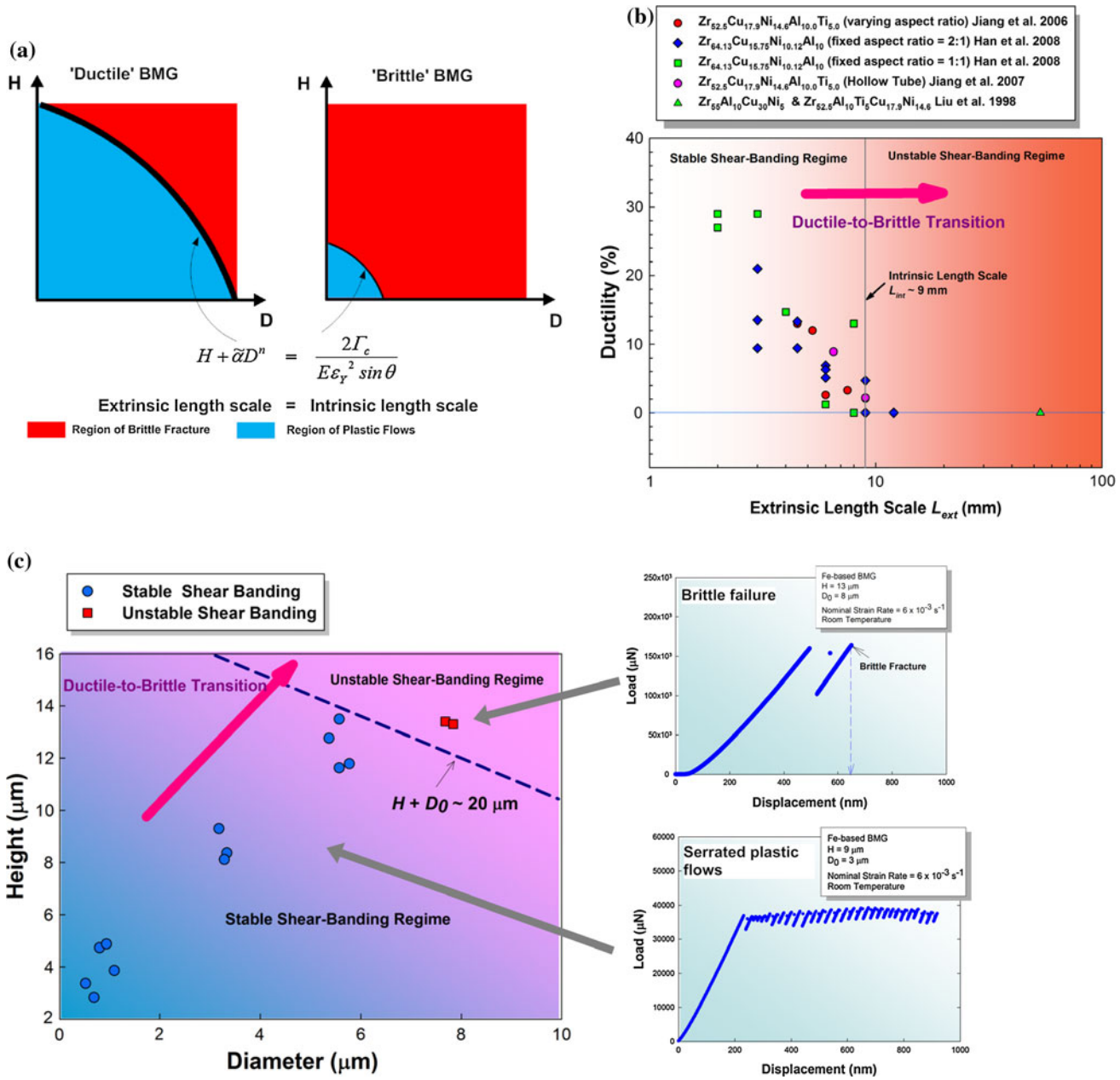

Fig. 9 **a** Comparison of ductile and brittle BMGs under compressive loading with the deformation mechanism map for size effect; **b** the variation of the experimentally measured compressive ductility of the Zr-based BMGs with the estimated extrinsic length scale, indicative of an intrinsic length scale around ~10 mm; and **c** the deformation mechanism map constructed from the microcompression of a Fe-based BMG showing an intrinsic length scale of ~20 μm. (Note that **b** is adapted from [29])

Different from the above reasoning, Lewandowski et al. proposed that the apparent brittleness and plasticity in BMGs should be correlated with their μ/B ratio or equivalently, their Poisson's ratio [70], where μ and B denote the shear and bulk modulus, respectively. According to the authors [70], such an idea originated from the behavior of crystalline materials, whose fracture mode is governed by the competition between cleavage fracture and dislocation emission. When the μ/B ratio exceeds a critical value, the material tends to fail in a brittle manner as its ability to resist bond breaking, which scales with B, is overweighed by that to dislocation emission, which scales with μ; conversely, it will fracture in a plastic manner if possessing a small μ/B ratio. As shown in Fig. 10, the experimental results showed a good correlation between the fracture toughness of BMGs and their μ/B ratios. However, as discussed previously, the failure mechanism in compression tests differs from that of fracture. The former is due to shear-band over-slip, while the latter to crack growth; therefore, it is unlikely

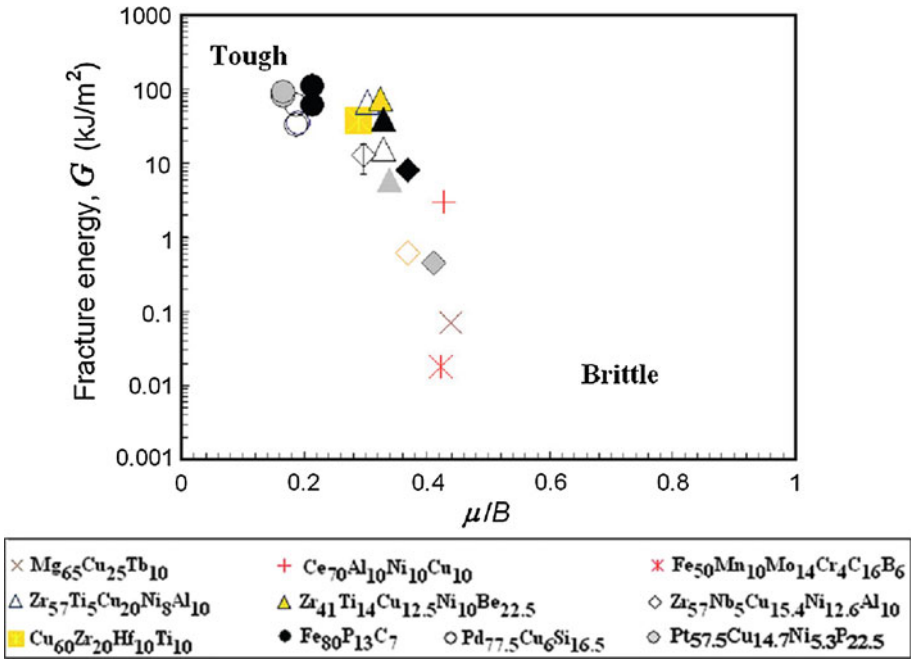

Fig. 10 The correlation of fracture energy G with elastic modulus ratio μ/B for the variety of as-cast BMGs as originally presented in Ref. [70]

that the same mechanism which governs the fracture of BMGs should be also applicable to that in uniaxial compressive loading. Furthermore, the size effect is also a strong proof that it is inappropriate to use the μ/B ratio as the sole parameter to infer the intrinsic brittleness/plasticity in BMGs [50].

Before ending this section, it is worth mentioning that the size-effect models developed so far has been mainly checked with the compression data [28, 29, 56, 60]. However, even the BMG possessing a great malleability shows limited or zero plasticity under tension [71]. Such a phenomenon of tension–compression asymmetry has been noted for many years [72], and could be apparently attributed to the stress effect on void growth in BMGs [63, 67, 73]. Under tensile loading, voids can easily grow in a shear band, causing premature fracture upon yielding; while under compressive loading, their growth is suppressed, leaving the opportunity for a shear band to propagate stably for serrated plastic flows. Bearing this in mind, it can be envisaged that there should be a competition of deformation mechanisms between shear-band slip and void growth in BMGs under tensile loading. For bulk samples, shear slip may be interrupted by shear-induced cracking, causing the material to fail in a brittle manner with a crack-like fracture morphology [67]; while for small samples, void growth may be retarded and therefore, a similar sample size effect on shear-band propagation as in compression tests rises again in tension tests [24, 40]. To fully understand the mechanism of deformation and fracture in BMGs under tensile loading, additional research efforts are still needed.

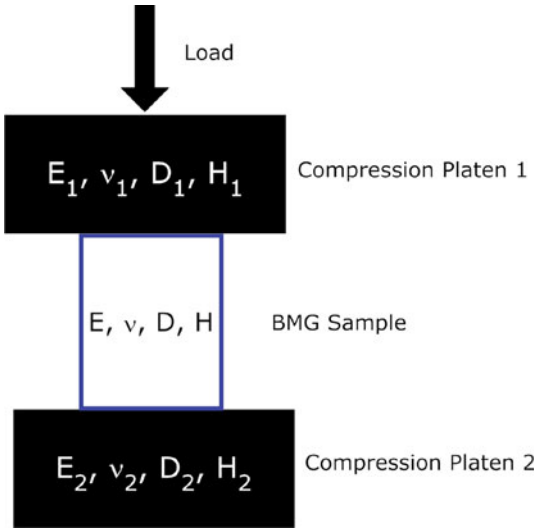

Fig. 11 The illustrated experimental set-up for a compression test on a BMG sample

Concluding remarks

As compared to their crystalline counterparts, BMGs gain their superb mechanical strength seemingly at the sacrifice of their ductility. Therefore, over the past years, tremendous research efforts have been devoted to finding a recipe that can make an intrinsically ductile BMG. However, through the recent research findings, it can be readily perceived that MGs are neither intrinsically brittle nor ductile, at least under compressive loading. The apparent brittleness usually witnessed at the macroscopic scale results from a shear-banding size effect, which can be

traced back to the multistep nature of shear banding in BMGs under compressive loading. While BMGs may display extensive plastic flows in a compression test when their size falls within the stable shear-banding region, however, it has been observed that most likely they still fracture in a brittle manner in a tension test. This tension–compression asymmetry is implicative of a stress state effect on shear-band propagation in BMGs, which remains as an open question that warrants further research.

Acknowledgements Y.Y. is grateful to the financial support provided by the Hong Kong Polytechnic University for newly recruited academic staff (project code G-YH85), and the Research Grant Council (RGC), the Hong Kong Government, through the General Research Fund (GRF) with a project number of PolyU 5359/09E. Y.Y. is thankful to the graduate student, J.C. Ye, for conducting and analyzing the data of the microcompression experiments on the Fe-based MG micropillars, from which Fig. 9c is generated.

Appendix: The α parameter and the extrinsic length scale L_{ext}

The theoretical derivation of the α parameter has been detailed in our recent work [60]. For the information of readers, the general expression for the α parameter is introduced here. According to the dimensional analysis, the α parameter can be expressed as follows for a cylindrical BMG sample compressed between two cylindrical compression platens:

$$\alpha = \left(\sum_{i=1}^{2} \Pi_i\left(\frac{D}{D_i}, \frac{H_i}{D_i}, v_i\right)\frac{E}{E_i}\right)\frac{\pi}{4} \tag{7}$$

where the symbols D, H, E, and v denote the object diameter, the object height, the Young's modulus, and the Poisson's ratio, respectively. For the BMG sample, those symbols carry no subscript; while for the compression platens, they are labeled with a subscript (1 = upper platen and 2 = lower platen), as shown in Fig. 11. Here Π represents a dimensionless function of which the exact functional form is not known yet.

For microcompression tests, the upper platen is a diamond punch that may be assumed as a rigid body ($E_1 = \infty$), and the lower one is the base material, which can be regarded as an elastic half infinite space ($D_1 = \infty$ and $H_1 = \infty$) and possesses the same material properties as the micropillar. In such a case, the functional form of the α parameter is reduced to $\alpha = \alpha(v)$, which only depends on the Poisson's ratio of the BMG. Through the FE simulation, one may fit the simulated values of the α parameter to a linear function, which reads $\alpha = 4(5.6 - 4v)/\pi$ [26]. Assuming an average Poisson's ratio of ~0.35 for BMGs, the α parameter can be then estimated as around ~5. As such, the corresponding extrinsic length scale L_{ext} can be expressed as $L_{ext} = H + 5D$.

For regular compression tests, the α parameter is a multivariable function. For simplicity, let us assume that both upper and lower platens are made of the same material and possess the same size and geometry ($E_1 = E_2$, $D_1 = D_2$, $H_1 = H_2$, and $v_1 = v_2$). As such, Eq. 7 can be simplified to:

$$\alpha = \Pi_1\left(\frac{D}{D_1}, \frac{H_1}{D_1}, v_1\right)\frac{E}{E_1}\frac{\pi}{2} \tag{8}$$

In principle, FE simulations can be performed to attain a proper functional form for Π_1 that fits the elastic boundary conditions set in a real experiment as seen in [26]. After that, the corresponding extrinsic length scale L_{ext} can be derived and then utilized for studying the size effect in a quantitative manner. Here, for the sake of demonstration, we assume the following functional form for Π_1 for a finite platen size without resorting to the FE simulations:

$$\Pi_1 = \left(\frac{D}{D_1}\right)^x\left(\frac{H_1}{D_1}\right)^y\frac{2f(v_1)}{\pi} \tag{9}$$

where the exponent x, y and the single-variable function f are to be fitted out by FE simulations. Substituting (9) into (3a) then gives the corresponding extrinsic length scale L_{ext}:

$$L_{ext} = H + \left(\frac{D}{D_1}\right)^{x-1}\left(\frac{H_1}{D_1}\right)^{y-1}\frac{\pi E}{4k_M}f(v_1)D^2 \tag{10}$$

in which $k_M = \pi E_1 D_1^2/4H_1$ is the machine stiffness. Now, if we further assume $x = y = f(v_1) = 1$, (10) is therefore simplified to:

$$L_{ext} = H + \frac{\pi E}{4k_M}D^2 \tag{11}$$

Comparing (11) to Eq. 2 in the main text, it can be easily seen that the general size-effect model described here is now reduced to the size-effect model developed by Cheng et al. [56] and their proposed shear-band instability index (S_{new}) is equivalent to the extrinsic length scale, L_{ext}, of a special form.

References

1. Klement W, Willens RH, Duwez P (1960) Nature 187:869
2. Ashby MF, Greer AL (2006) Scripta Mater 54:321
3. Lu ZP, Liu CT (2004) J Mater Sci 39:3965. doi:10.1023/B:JMSC.0000031478.73621.64
4. Waseda Y, Aust KT (1981) J Mater Sci 16:2337. doi:10.1007/BF01113569
5. Davis LA (1975) J Mater Sci 10:1557. doi:10.1007/BF01031856

6. Schuh CA, Hufnagel TC, Ramamurty U (2007) Acta Mater 55:4067
7. Zhang Y, Greer AL (2006) Appl Phys Lett 89:071907
8. Jiang MQ, Wang WH, Dai LH (2009) Scripta Mater 60:1004
9. Liu YH, Liu CT, Gali A, Inoue A, Chen MW (2010) Intermetallics 18:1455
10. Yang Y, Ye JC, Lu J, Wang Q, Liaw PK (2010) J Mater Res 25:563
11. Guo H, Wen J, Xiao NM, Zhang ZF, Sui ML (2008) J Mater Res 23:2133
12. Spaepen F (1977) Acta Metall 25:407
13. Argon AS (1979) Acta Metall 27:47
14. Ye JC, Lu J, Liu CT, Wang Q, Yang Y (2010) Nat Mater 9:619
15. Hirata A, Guan PF, Fujita T, Hirotsu Y, Inoue A, Yavari AR, Sakurai T, Chen MW (2010) Nat Mater 10:28
16. Gao YF (2006) Model Simul Mater Sci Eng 14:1329
17. Homer ER, Rodney D, Schuh CA (2010) Phys Rev B 81:064204
18. Lewandowski JJ, Greer AL (2006) Nat Mater 5:15
19. Wright WJ, Schwarz RB, Nix WD (2001) Mater Sci Eng A 319–321:229
20. Yang B, Liu CT, Nie TG, Morrison ML, Liaw PK, Buchanan RA (2006) J Mater Res 21:915
21. Wright JL, Samale MW, Hufnagel TC, LeBlanc MM, Florando JN (2009) Acta Mater 57:4639
22. Chen HM, Huang JC, Song SX, Nieh TG, Jang JSC (2009) Appl Phys Lett 94:141914
23. Zhao M, Li M (2009) J Mater Res 24:2688
24. Wu FF, Zhang ZF, Mao SX (2009) Acta Mater 57:257
25. Wu FF, Zhang ZF, Shen BL, Mao SXY, Eckert J (2008) Adv Eng Mater 10:727
26. Ye JC, Lu J, Yang Y, Liaw PK (2009) Acta Mater 57:6037
27. Chen CQ, Hosson JTMD (2010) Acta Mater 58:189
28. Han Z, Wu WF, Li Y, Wei YJ, Gao HJ (2009) Acta Mater 57:1367
29. Yang Y, Ye JC, Lu J, Liaw PK, Liu CT (2010) Appl Phys Lett 96:011905
30. Egami T (2010) JOM-US 62:70
31. Sheng HW, Luo WK, Alamgir FM, Bai JM, Ma E (2006) Nature 439:419
32. Miracle DB (2004) Nat Mater 3:697
33. Fan C, Liaw PK, Wilson TW, Dmowski W, Choo H, Liu CT, Richardson JW, Proffen T (2006) Appl Phys Lett 89:111905
34. Fan C, Liaw PK, Liu CT (2009) Intermetallics 17:86
35. Fan C, Ren Y, Liu CT, Liaw PK, Yan HG, Egami T (2011) Phys Rev B 83:195207
36. Cheng YQ, Ma E (2011) Prog Mater Sci 56:379
37. Gao YF, Yang B, Nieh TG (2007) Acta Mater 55:2319
38. Yang Y, Ye JC, Lu J, Gao YF, Liaw PK (2010) Jom 62:93
39. Cheng YQ, Ma E (2011) Acta Mater 59:1800
40. Guo H, Yan PF, Wang YB, Tan J, Zhang ZF, Sui ML, Ma E (2007) Nat Mater 6:735
41. Jang DC, Greer JR (2010) Nat Mater 9:215
42. Volkert CA, Donohue A, Spaepen F (2008) J Appl Phys 103:083539
43. Schuster BE, Wei Q, Hufnagel TC, Ramesh KT (2008) Acta Mater 56:5091
44. Wu XL, Guo YZ, Wei Q, Wang WH (2009) Acta Mater 57:3562
45. Ye JC, Lu J, Yang Y, Liaw PK (2009) J Mater Res 24:3465
46. Schuh CA, Nieh TG (2004) J Mater Res 19:46
47. Song SX, Bei H, Wadsworth J, Nie TG (2008) Intermetallics 16:813
48. Demetriou MD, Veazey C, Harmon JS, Schramm JP, Johnson WL (2008) Phys Rev Lett 101:145702
49. Yu HB, Hu J, Xia XX, Sun BA, Li XX, Wang WH, Bai HY (2009) Scripta Mater 61:640
50. Gu XJ, Poon SJ, Shiflet GJ, Lewandowski JJ (2010) Acta Mater 58:1708
51. Xie S, George EP (2008) Intermetallics 16:485
52. Vinogradov A (2010) Scripta Mater 63:89
53. Dalla Torre FH, Klaumunzer D, Maass R, Loffler JF (2010) Acta Mater 58:3742
54. Packard CE, Schuh CA (2007) Acta Mater 55:5348
55. Cao AJ, Cheng YQ, Ma E (2009) Acta Mater 57:5146
56. Cheng YQ, Han Z, Li Y, Ma E (2009) Phys Rev B 80:134115
57. Wu FF, Zhang ZF, Mao SX, Eckert J (2009) Philos Mag Lett 89:178
58. Wu WF, Han Z, Li Y (2008) Appl Phys Lett 93:061908
59. Wu Y, Li HX, Jiao ZB, Gao JE, Lu ZP (2010) Philos Mag Lett 90:403
60. Yang Y, Ye JC, Lu J, Liu CT (2011) Intermetallics 19:1005
61. Wu Y, Li HX, Liu ZY, Chen GL, Lu ZP (2010) Intermetallics 18:157
62. Johnson WL, Samwer K (2005) Phys Rev Lett 95:195501
63. Zhang ZF, Eckert J, Schultz L (2003) Acta Mater 51:1167
64. Greer AL (2009) Mater Today 12:14
65. Zhang H, Maiti S, Subhash G (2008) J Mech Phys Solids 56:2171
66. Miracle DB, Concustell A, Zhang Y, Yavari AR, Greer AL (2011) Acta Mater 59:2831
67. Liu CT, Heatherly L, Easton DS, Carmichael CA, Schneibel JH, Chen CH, Wright JL, Yoo MH, Horton JA, Inoue A (1998) Metall Mater Trans A 29A:1811
68. Sun L, Jiang MQ, Dai LH (2010) Scripta Mater 63:945
69. Liu YH, Liu CT, Wang WH, Inoue A, Sakurai T, Chen MW (2009) Phys Rev Lett 103:065504
70. Lewandowski JJ, Wang WH, Greer AL (2005) Philos Mag Lett 85:77
71. Yokoyama Y, Fujita T, Yavari AR, Inoue A (2009) Phill Mag Lett 89:322
72. Pampillo CA (1975) J Mater Sci 10:1194. doi:10.1007/BF00541403
73. Wright WJ, Hufnagel TC, Nix WD (2003) J Appl Phys 93:1432